The ASTRI Mini-Array view of the Cygnus region

Antonino D'Aì

A. Tutone, L.Barrios-Jimenez, M. Cardillo, A. Compagnino, S. Crestan, A.Giuliani,
S. Lombardi, F. Pintore, M. Rigoselli on behalf for the ASTRI Project

8th Heidelberg International Symposium on High-Energy Astrophysics, Milan, 2-6 September 2024

Aims of this presentation

- Introduce the forthcoming ASTRI Mini-Array and present expected performance in terms of sensitivity, energy and spatial resolution.
- Introduce the concept of the scientific pillars and general observational strategies.
- Present the Cygnus Data Challenge: observing strategy, pipeline developments, the sky model and some scientific results.

ASTRI Mini-Array

ASTRI-MA sensitivity and characteristics in comparison with existing IACTs

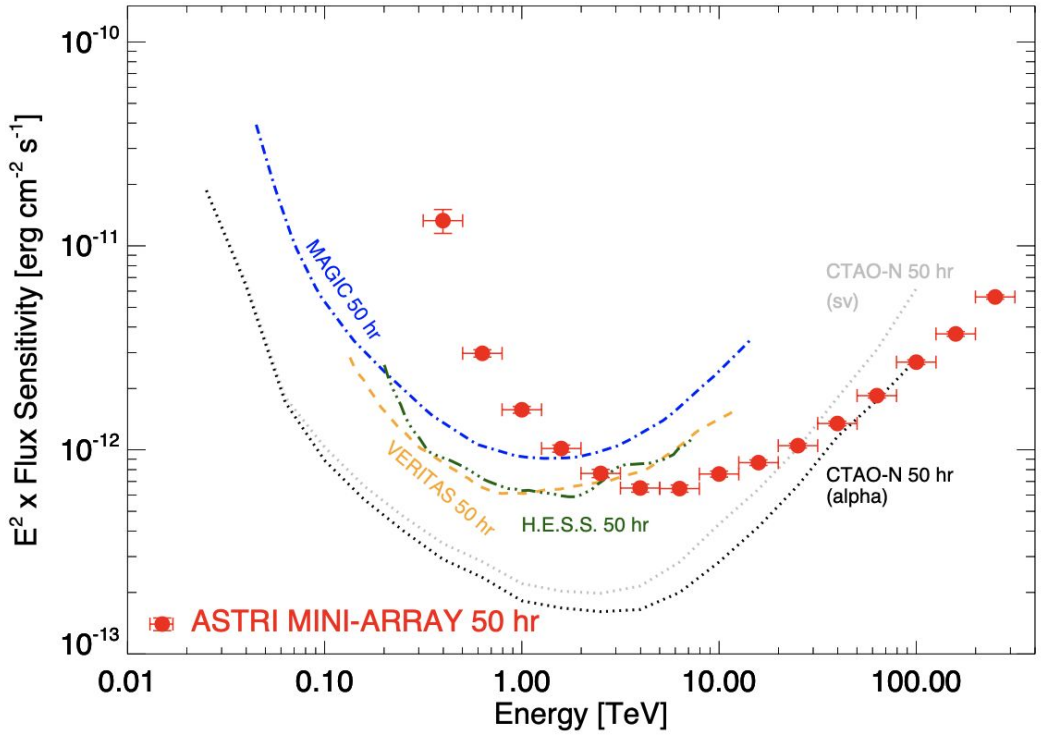

	ASTRI Mini-Array	MAGIC	VERITAS	H.E.S.S.
Location	28° 18′ 04″ N	28° 45′ 22″ N	31° 40′ 30″ N	23° 16′ 18″ S
	16° 30′ 38″ W	17° 53′ 30″ W	110° 57′ 7.8″ W	16° 30′ 00″ E
Altitude [m]	2,390	2,396	1,268	1,800
FoV	~10°	~3.5°	~3.5°	~5°
Angular Res.	0.05° (30 TeV)	0.07° (1 TeV)	0.07° (1 TeV)	0.06° (1 TeV)
Energy Res.	12% (10 TeV)	16% (1 TeV)	17% (1 TeV)	15% (1 TeV)
Energy Range	(0.3-200) TeV	(0.05-20) TeV	(0.08-30) TeV	(0.02-30) TeV$^{(\alpha)}$

See also C.Bigongiari talk Friday @this conference

Vercellone, PoS, 2022

ASTRI Mini-Array

ASTRI-MA sensitivity and characteristics in comparison with other gamma-ray facilities

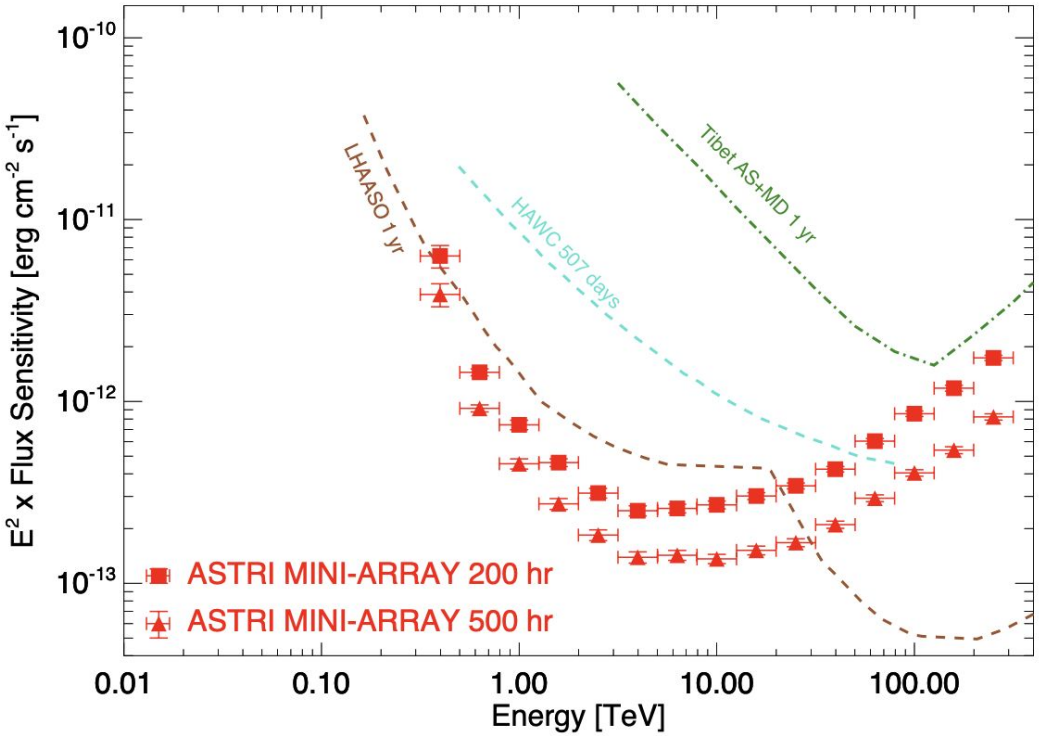

	ASTRI Mini-Array	HAWC	LHAASO	Tibet ASγ
Location	28° 18′ 04″ N 16° 30′ 38″ W	18° 59′ 41″ N 97° 18′ 27″ W	29° 21′ 31″ N 100° 08′ 15″ E	30° 05′ 00″ N 90° 33′ 00″ E
Altitude [m]	2,390	4,100	4,410	4,300
FoV	~10°	2 sr	2 sr	2 sr
Angular Res.	0.05° (30 TeV)	0.15°[a] (10 TeV)	(0.24–0.32)°[b] (100 TeV)	0.2°[c] (100 TeV)
Energy Res.	12% (10 TeV)	30% (10 TeV)	(13–36)% (100 TeV)[b]	20%[c] (100 TeV)
Energy Range	(0.3-200) TeV	(0.1-1000) TeV	(0.1-1000) TeV	(0.1-1,000) TeV

Vercellone, PoS, 2022

The Science Pillars

- In the first four years, ASTRI Mini-Array will operate as an experiment. Scientific schedule will privilege long-exposure observations of selected sky fields.
- The “pillars” of this investigation fall into these main scientific areas:
  - Origin of cosmic rays (PeVatrons, PWN acceleration mechanisms)
  - Fundamental physics (Cosmology, EBL, dark matter)
  - The Transient and multi-messenger sky (GRBs, GWs)

Vercellone et al., 2022, JHEP, 35, 1-42

The Science Pillars

- In the first four years, ASTRI Mini-Array will operate as an experiment. Scientific schedule will privilege long-exposure observations of selected sky fields.
- The “pillars” of this investigation fall into these main scientific areas:
  - Origin of cosmic rays (PeVatrons, PWN acceleration mechanisms)
  - Fundamental physics (Cosmology, EBL, dark matter)
  - The Transient and multi-messenger sky (GRBs, GWs)

Vercellone et al., 2022, JHEP, 35, 1-42

However, ongoing discoveries offer the opportunity to re-address the best candidate sources to tackle such questions.

The densest TeV source region

The Cygnus region is comprised between 64-84 deg in Galactic longitude and +/- 3 deg in latitude. It is the most crowded and scientifically reach TeV field in the Northern sky.

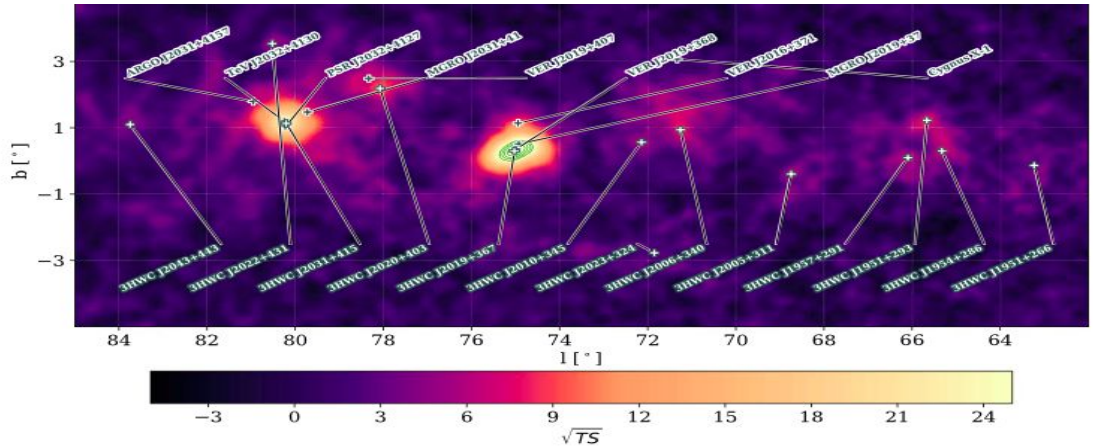

[Third HAWC catalogue]

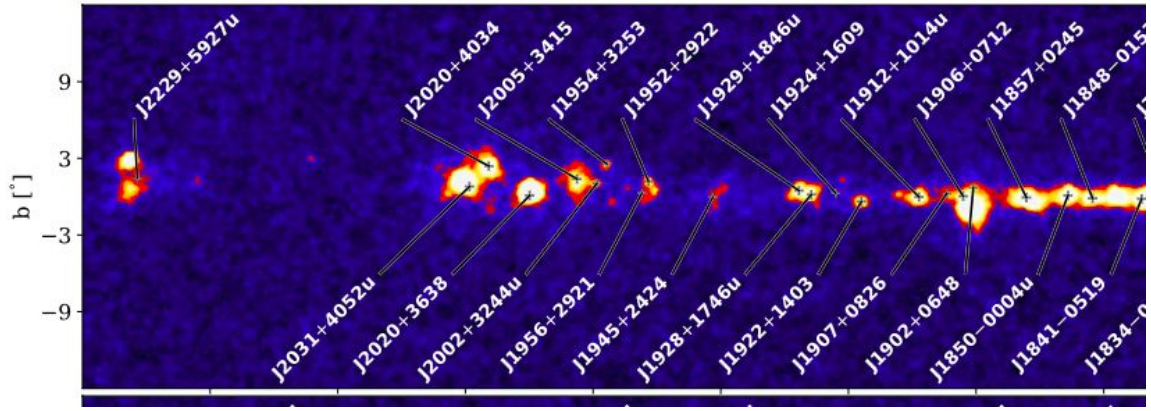

[First LHAASO catalogue.]

43 sources detected >100 TeV

The Cygnus region

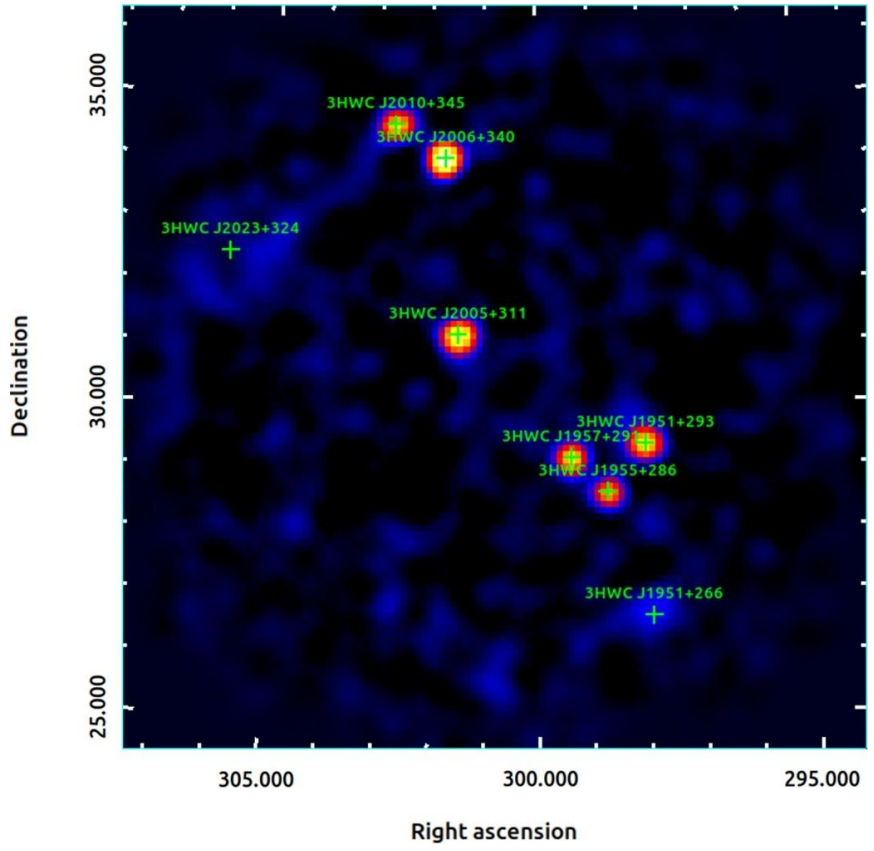

Simulation with 200 hr of uniform exposure (Vercellone, 2022)

A test on detection capabilities as function of exposure times.
We included only HAWC third catalogue sources.
Simplified spectral/spatial modelling.
No diffuse emission.
No realistic pointing strategy.

D'Aì et al. 2022, JHEAP, 35, 139


Contents lists available at ScienceDirect

Journal of High Energy Astrophysics

www.elsevier.com/locate/jheap

Galactic observatory science with the ASTRI Mini-Array at the *Observatorio del Teide*

A. D'Aì [a,*], E. Amato [b], A. Burtovoi [b], A.A. Compagnino [a], M. Fiori [c], A. Giuliani [d], N. La Palombara [d], A. Paizis [d], G. Piano [e], F.G. Saturni [f,g], A. Tutone [a,h], A. Belfiore [d], M. Cardillo [e], S. Crestan [d], G. Cusumano [a], M. Della Valle [i,j], M. Del Santo [a], A. La Barbera [a], V. La Parola [a], S. Lombardi [f,g], S. Mereghetti [d], G. Morlino [b], F. Pintore [a], P. Romano [k], S. Vercellone [k], A. Antonelli [f], C. Arcaro [l], C. Bigongiari [f,g], M. Böettcher [m], P. Bruno [n], A. Bulgarelli [o], V. Conforti [o], A. Costa [n], E. de Gouveia Dal Pino [p], V. Fioretti [o], S. Germani [q], A. Ghedina [r], F. Gianotti [o], V. Giordano [n], F. Incardona [n], G. Leto [n], F. Longo [s,t], A. López Oramas [u], F. Lucarelli [f,g], B. Olmi [v], A. Pagliaro [a], N. Parmiggiani [o], G. Romeo [n], A. Stamerra [f], V. Testa [f], G. Tosti [o,q], G. Umana [n], L. Zampieri [e], P. Caraveo [d], G. Pareschi [k]

Realistic pointing plan

Sky visibility from Teide

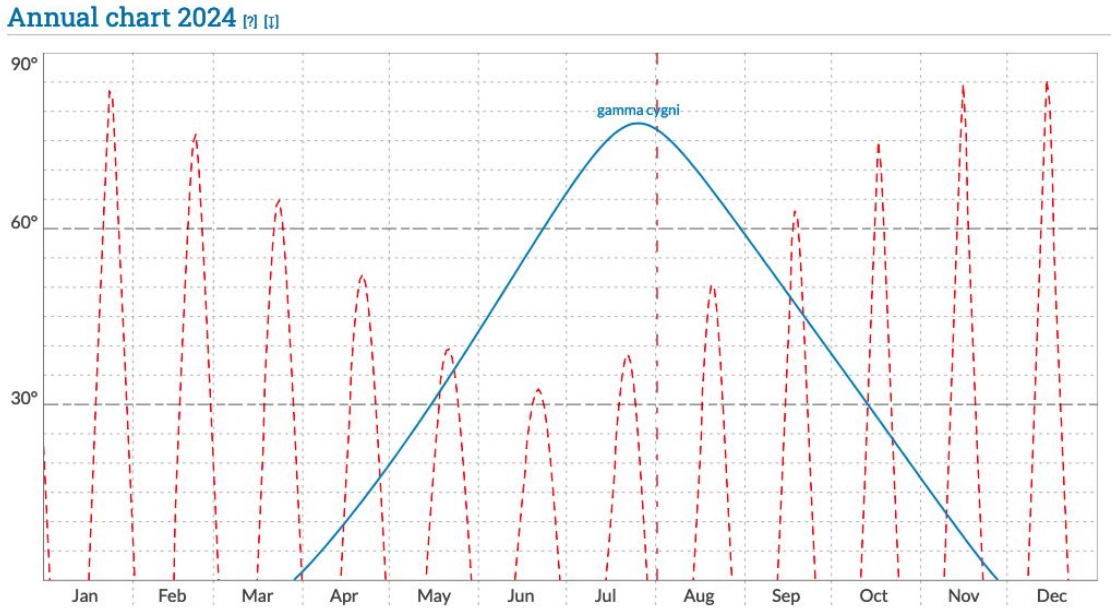

540 hours of net exposure divided in 180 pointings.

Realistic pointing plan

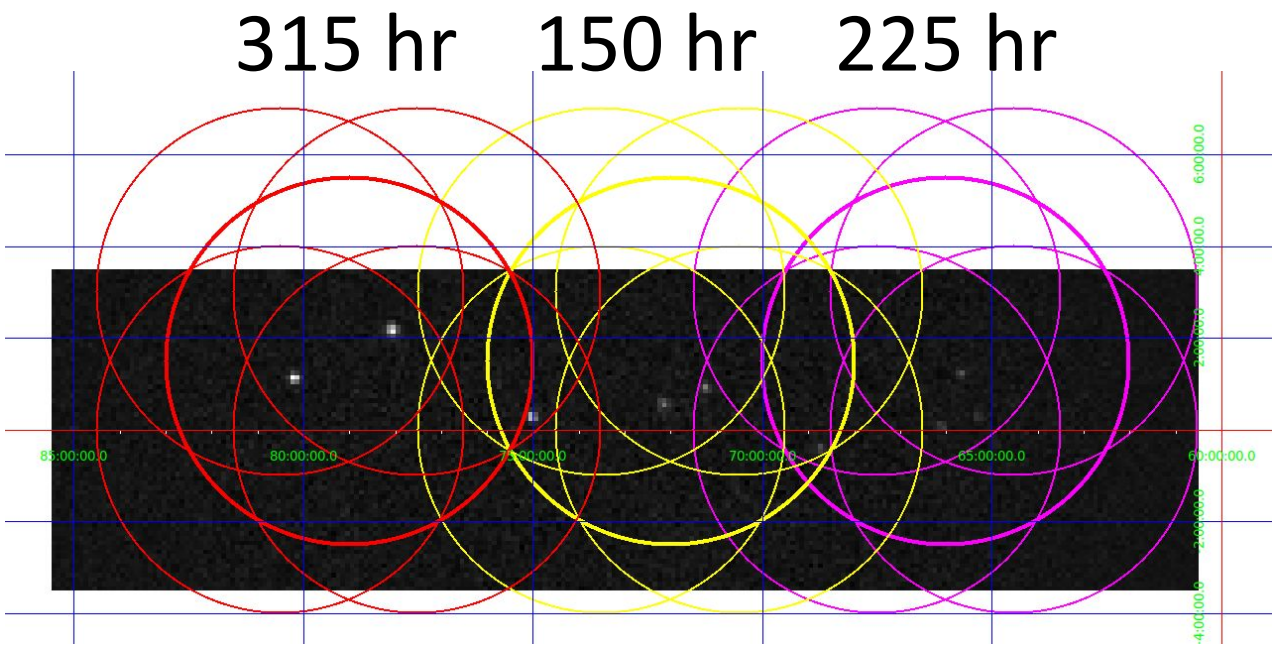

Modified double-rows.
Main pointings on the same Gal. latitude=1.5 deg, different Gal. longitudes (66,72,and 78 deg)

4-tiles separated by 1.5 deg in lat and in long with respect to the central position.

The tiling is not specular wrt the diffuse Galactic ridge emission, because sources of interest are mostly above the Galactic plane.

The DC Cygnus model ingredients

- Galactic ridge diffuse emission
- Point and extended sources from LHAASO/HAWC/MAGIC and VERITAS detections (13 sources)
- Cygnus bubble (from HAWC analysis)
- Irreducible background

A.Donath et al. 2023, A&A

Publicly available ASTRI-MA IRF @Zenodo
https://zenodo.org/records/6827882

Source TM	SpatialModel	SpectralModel
3HWC J1951+293	Point	Template
3HWC J1951+266	Disk	Template
3HWC J2005+311	Point	Template
3HWC J2006+340	Point	Template
3HWC J2010+345	Point	Template
3HWC J2022+431	Point	Template
3HWC J2023+324	Disk	Template
3HWC J2043+443	Disk	Template
LHAASO J2032+4102	Gaussian	ExpCutoffPowerLaw
PSR 2032	Disk	LogParabola
PSR J1954+2836	Gaussian	LogParabola
PSR J1958+2846	Gaussian	LogParabola
VER J2016+371	Template	ExpCutoffPowerLaw
VER J2018+367	Template	ExpCutoffPowerLaw
VER J2019+407	Template	Template
VER J2020+368	Template	ExpCutoffPowerLaw
fermi bubble	Gaussian	Template
diffuse BKG	Template	PowerLawNorm

The Cygnus Superbubble

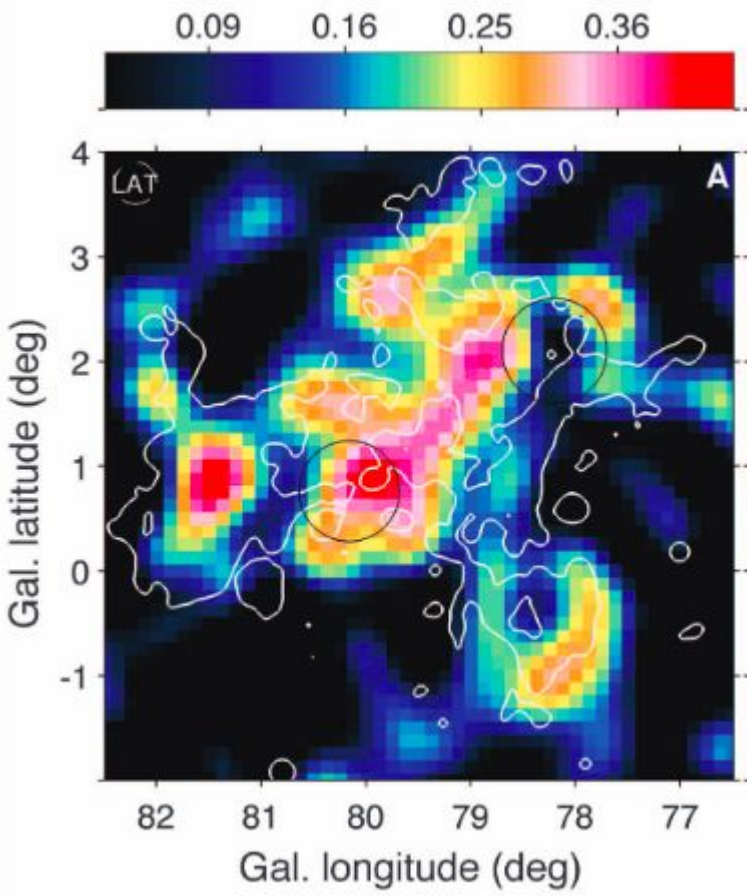

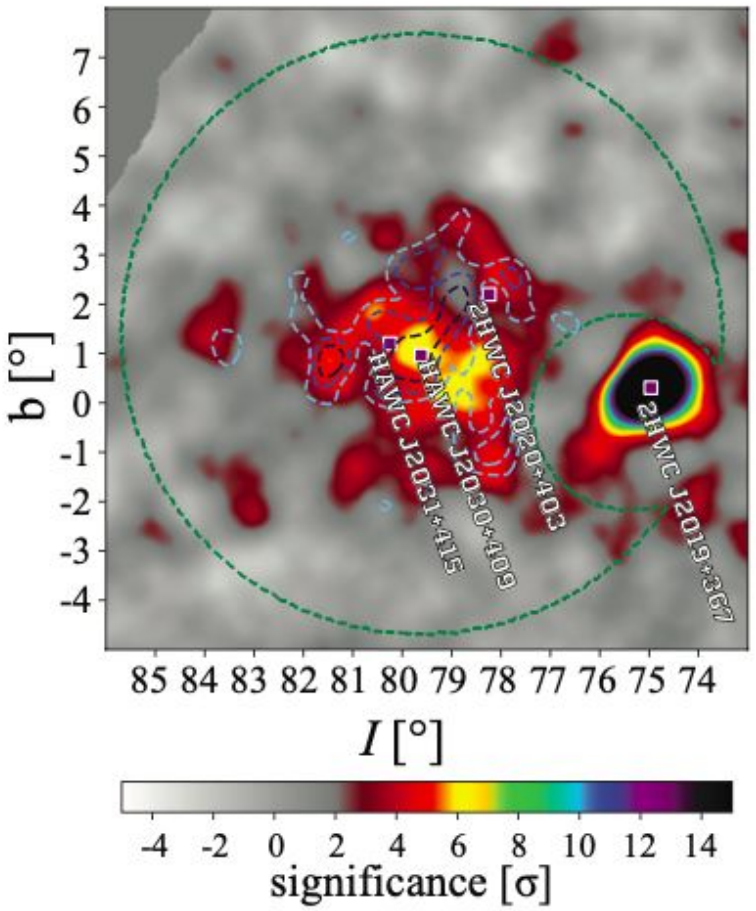

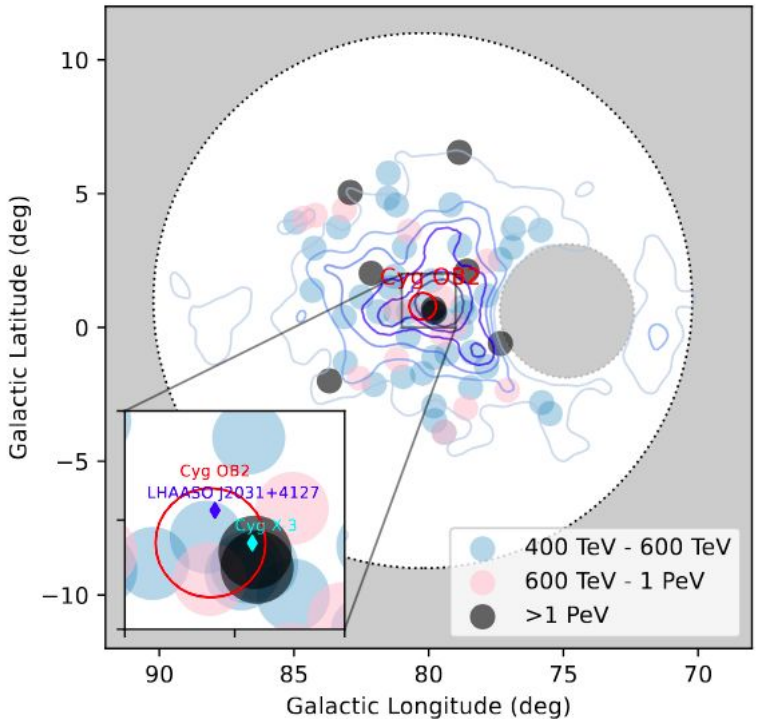

[Fermi Coll. 2011]

[HAWC Coll. 2021]

[LHAASO Coll. 2024]

The Cygnus Superbubble: spatial constraints

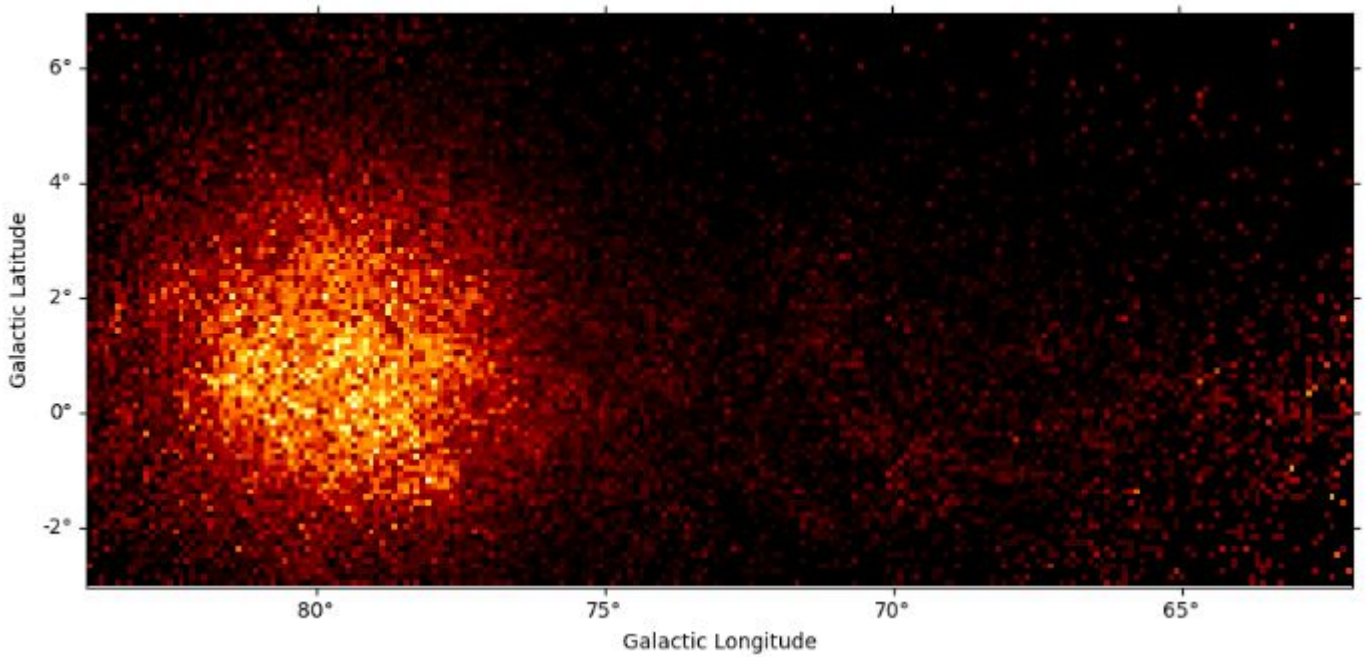

Thanks to @Antonio Tutone

Template: GaussianSpatialModel (lon=79.6°, lat=0.96°, σ=2.13°).

We sliced the region into rectangular subregions of 2.5deg width and applied a sliding window pace of 0.5 deg. Exposure-corrected counts per slice were fitted with a Gaussian profile.

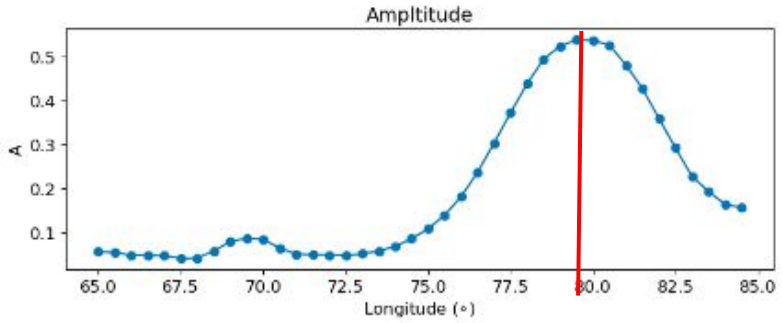

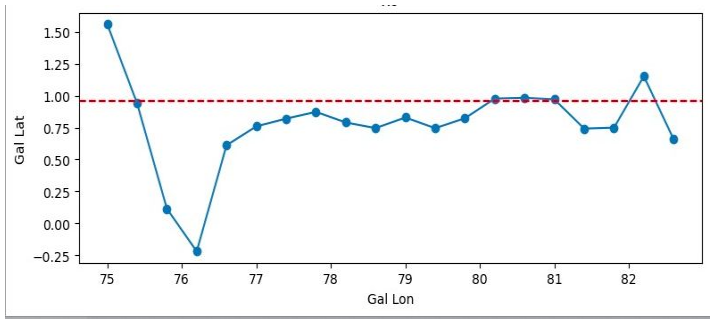

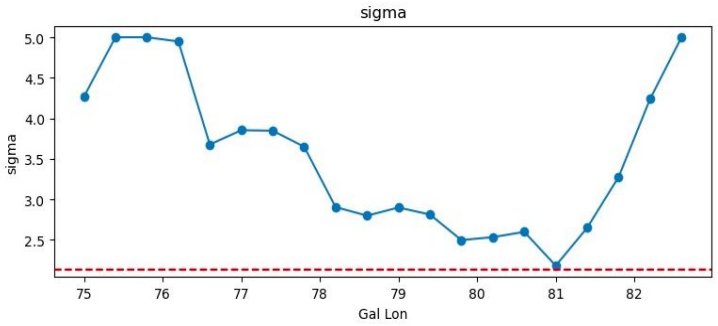

Spectral-spatial fit results

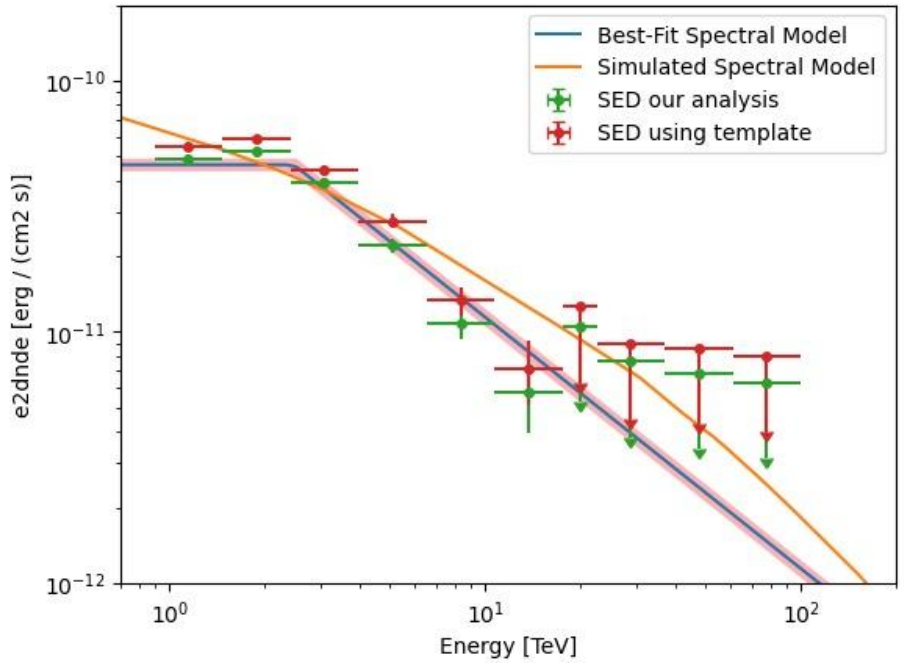

Spectral Models	Spatial Models	TS
PowerLaw	Disk	1153
	Gaussian	1294
ExponentialCutOffPwl	Disk	1204
	Gaussian	1356
LogParabola	Disk	1246
	Gaussian	1406
BrokenPowerLaw	Disk	1266
	Gaussian	1434

Uncertainties on the total flux determination driven by uncertainties in the sigma value of the spatial model and pivot @1TeV. This leads to overall flux uncertainty around 20 %.

The embedded PeVatron: LHAASO J2032+4102.

LHAASO J2032+4102 is embedded in the Fermi bubble, the most energetic PeVatron in the whole region. Confirmed also by Tibet ASGamma. Likely associated with the a massive star cluster (Cygnus OB1).

First LHAASO catalogue reported two sources at close distance, the same is reported by HAWC.

IACTs (MAGIC, VERITAS) reported only 3-4% C.U. flux from this location, associated with the PWN PSR J2032+4127 (which is also a gamma-ray binary !).

We simulated two extended sources of different spectral shapes (one softer, cut-off at 20 TeV) and one much harder (using Tibet Asgamma best-fit model).

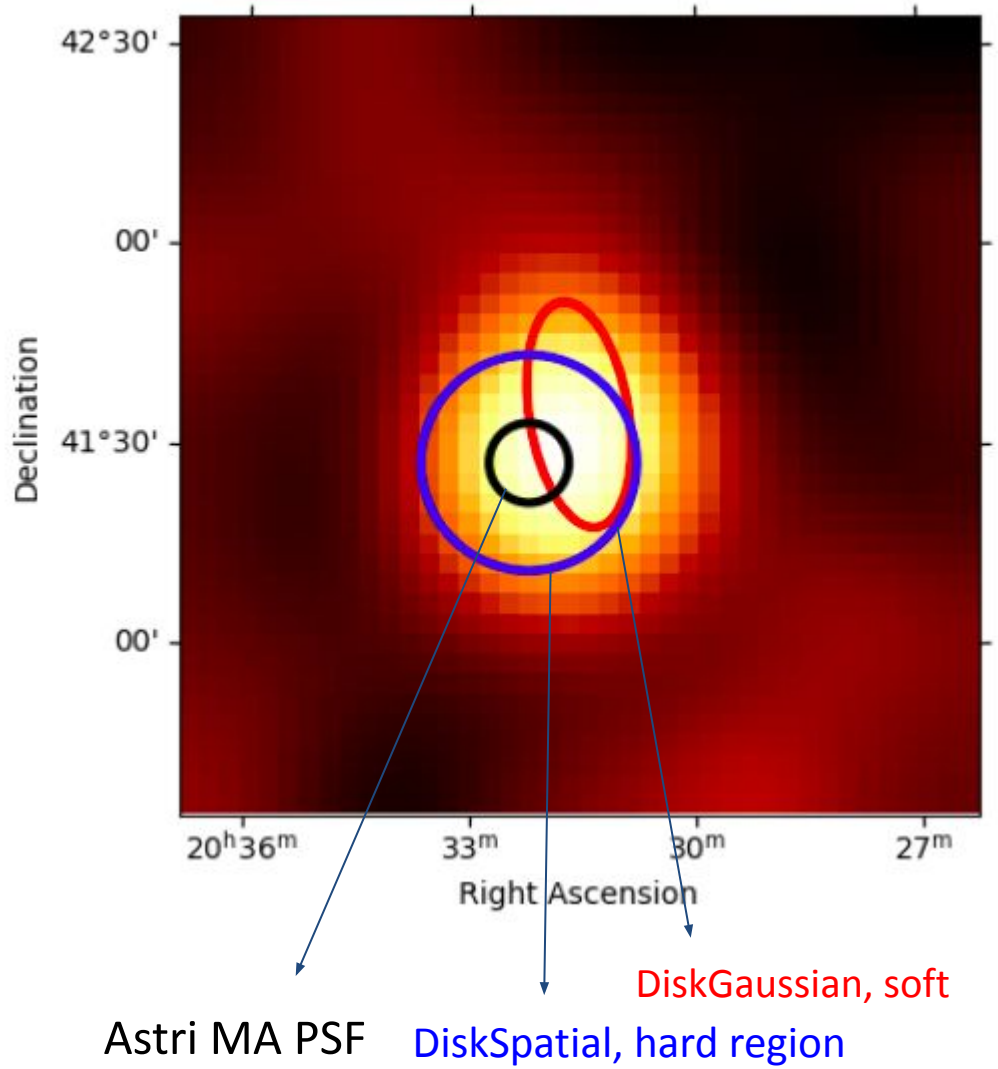

The embedded PeVatron: LHAASO J2032+4102.

ASTRI-MA is able to clearly distinguish the two regions as morphologically different.

The flux and spectral shapes were found consistent with the template model and the cut-off at 20 TeV of the softer region is well constrained. The hard region is detected above 100 TeV

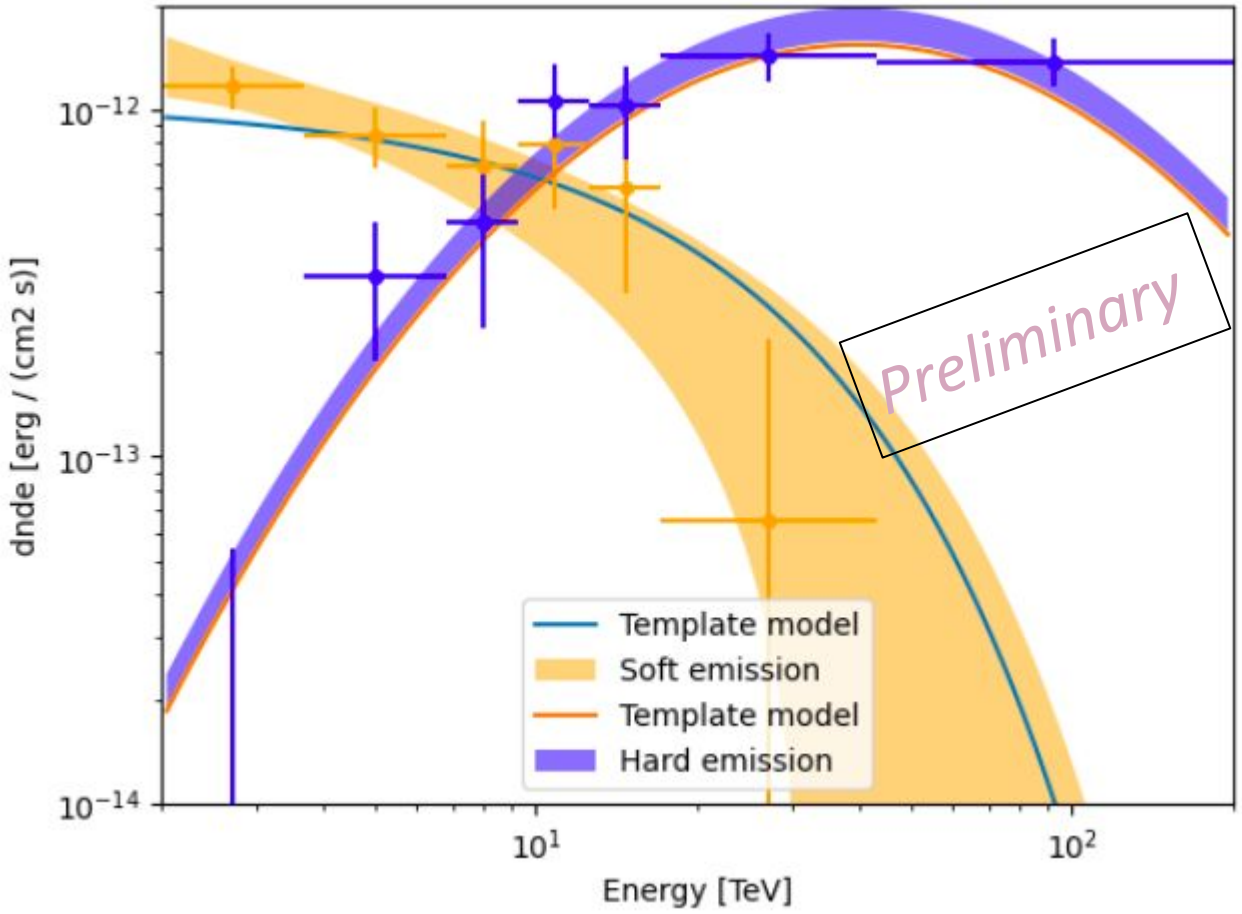

A pipeline for automatic source detection

An automated blind detection and source modelling pipeline based on Gammapy (developed by **Luis Barrios-Jiménez**)

Iterative approach:

1. First scan with Excess Peak.
2. Find if there are **overlapping sources.**
3. Model isolated and overlapping sources, deciding on extended single source or two separate sources.
4. Scan again, build the catalogue.

Source confusion

★ 2 sources are overlapping if:

$$d_{1,2}(^\circ) < 2\sigma_1 + 2\sigma_2 + 0.15^\circ$$

where σ_i is the std deviation of the spatial model

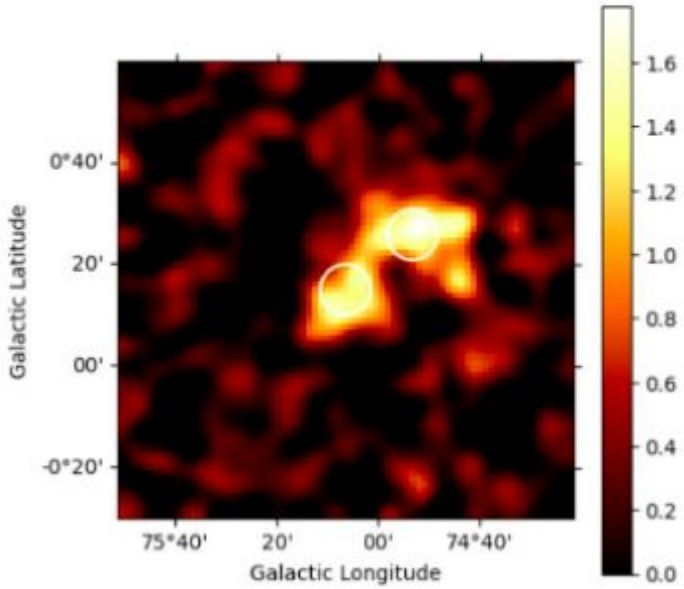

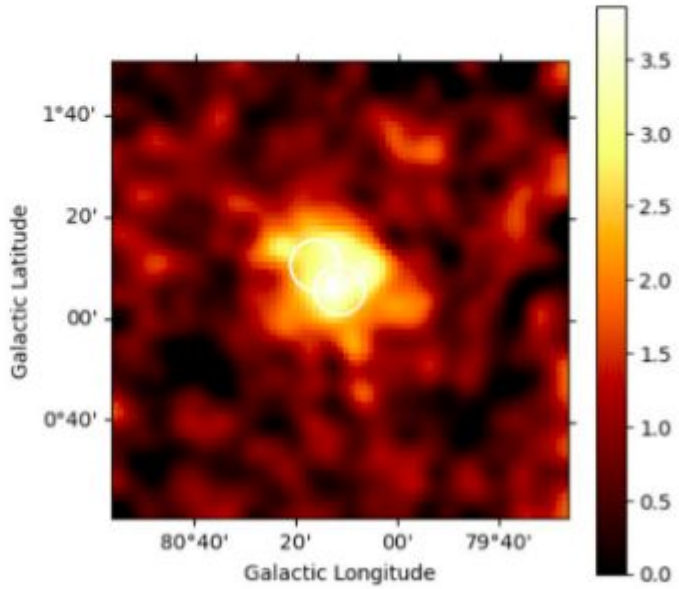

8

Results

Mini-Array

★ 11/14 sources detected with a significance above 5 σ

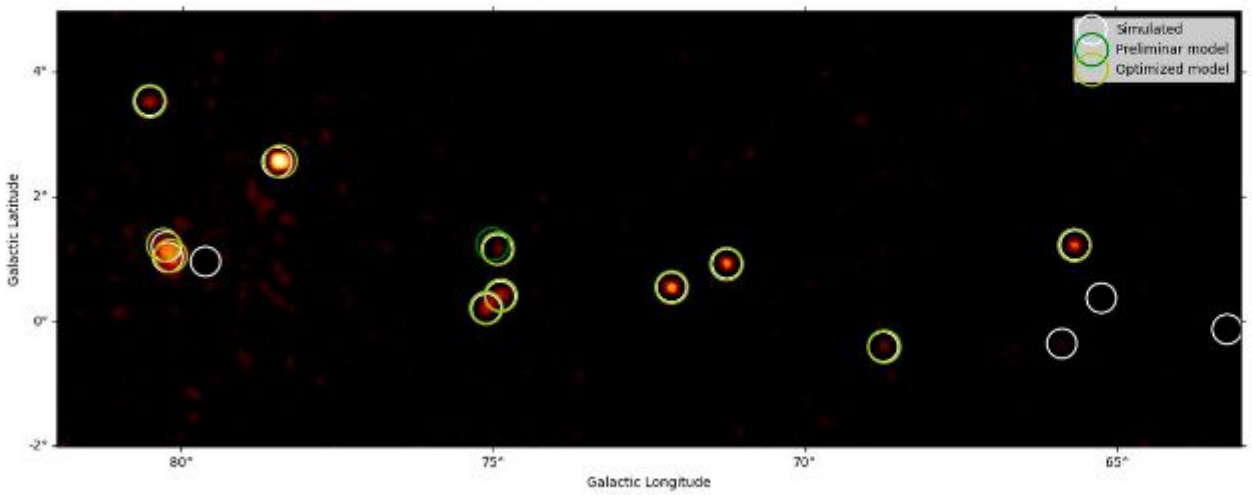

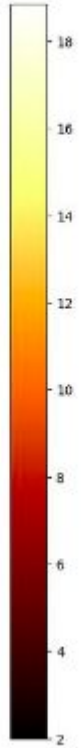

★ 10/8 point-like sources.

★ 1/6 extended sources

★ The 3 non-detected sources (2 extended) lie on a region with low exposure.

★ Positions are compatible with the simulated ones.

$\mu_{df,s}$ = 0.01 +- 0.03

Take-home messages

- ASTRI MA large FoV is perfectly suited for Galactic disk surveys, and the Cygnus region is the most promising field to be observed.
- ASTRI MA will be able to deliver spectro-morphological constraints on the growing population of ultra high-energy Galactic PeVatrons.
- The Cygnus DC allowed us to develop pipelines and tools for source determination and study of very extended structures like the Fermi SB.
- The determination of extended morphologies, which internally host a population of energetic local sources, will still be a challenging task.

Back-up slides

Fit details: spatial models

Parameter	Template	Fitted Parameter	Uncertainty (sigmas)
lon_0	80.224	80.21 ± 0.03	<1
lat_0	1.03	1.024 ± 0.005	1.2
r_0	0.27	0.272 ± 0.003	<1
lon_0	80.247	80.22 ± 0.03	<1
lat_0	1.2	1.18 ± 0.02	1
sigma	0.19	0.22 ± 0.02	1.5

Fit details: spectral models

Parameter	Template	Fitted Parameter	Uncertainty (sigmas)
index	2	2.1±0.4	<1
amplitude	1.24e-13	(1.7±0.3)e-13	1.5
lambda_	0.05	0.06±0.05	<1
amplitude	6e-16	(7±0.8)e-16	1.1
alpha	2	(1.8±0.2)	1

LHAASO J2032

Mini-Array

Source Name	Components	α_{2000}	δ_{2000}	$\sigma_{p,95,stat}$	r_{39}	TS	N_0	Γ	TS_{100}	Assoc. (Sep. (deg))
1LHAASO J2031 +4052u*	WCDA	307.90	40.88	0.19	0.25 ± 0.05	57.8	0.77 ± 0.12	2.81 ± 0.16		LHAASO J2032 +4102 (0.20)
	KM2A	308.14	40.88	0.13	<0.08	33.6	0.08 ± 0.02	2.13 ± 0.27	38.4	
1LHAASO J2031 +4127u	KM2A	307.95	41.46	0.03	0.22 ± 0.01	1953.6	2.56 ± 0.08	3.45 ± 0.06	136.9	TeV J2032 +4130 (0.12)
	WCDA	307.85	41.60	0.04	0.27 ± 0.01	1521.0	3.07 ± 0.12	2.29 ± 0.03		

Amenomori21

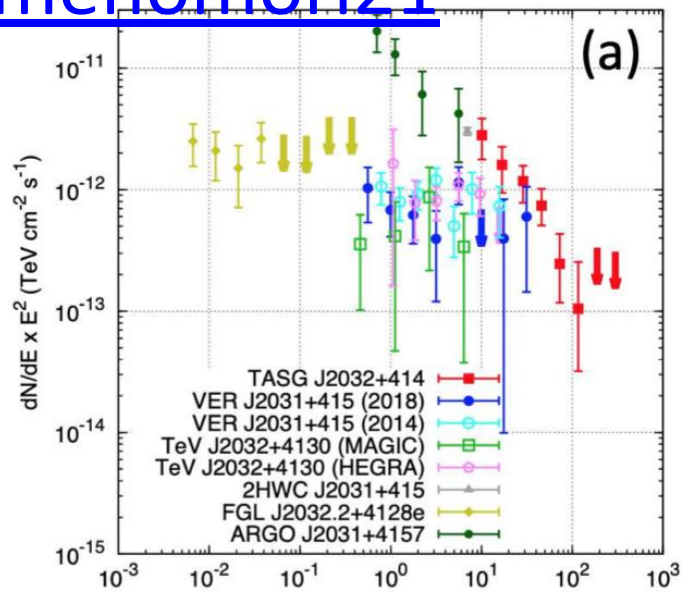

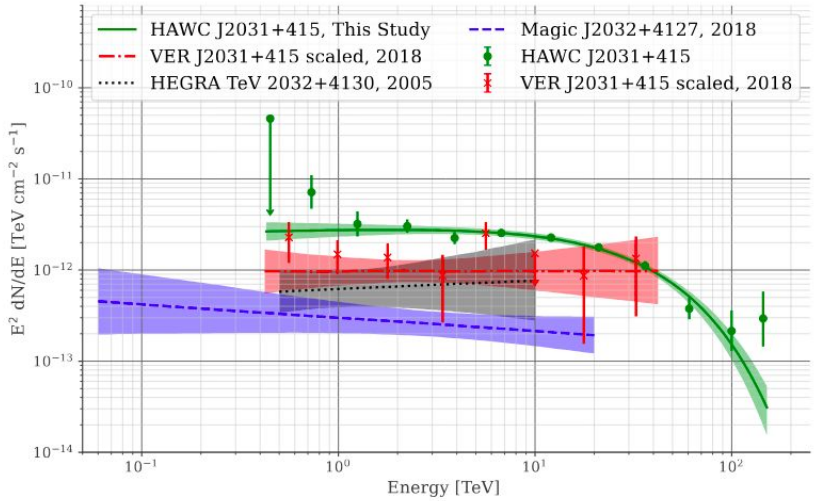

Figure 2. SED of HAWC J2031+415. The other observations are from Aharonian et al. (2005); Albert et al. (2008); Abeysekara et al. (2018b,a) respectively and were selected as the most current independent observations available. Additionally, all uncertainties are statistical only

Alfaro24